



NASA-CR-200150

*IN-20-CR
COVERPAGE*

7987

P. 7

AIAA 95-2725

Space Shuttle Solid Rocket Motor

Slag Expulsion Mechanisms

C. Hopson

Rockwell Aerospace

Huntsville, Al

**31st AIAA/ASME/SAE/ASEE
Joint Propulsion Conference and Exhibit
July 10-12, 1995/San Diego, CA**

SPACE SHUTTLE SOLID ROCKET MOTOR SLAG EXPULSION MECHANISMS

Charles B. Hopson*
Rockwell Aerospace, Huntsville, Alabama

A 13 psi pressure perturbation occurred at approximately 68 seconds on the right Redesigned Solid Rocket Motor (RSRM) during the STS-54 Space Shuttle mission. While pressure perturbations are a normal characteristic of RSRM operation, the magnitude of the STS-54 perturbation and the resulting thrust imbalance between the left and right motors was outside of flight experience. A joint Marshall Space Flight Center (MSFC) and Thiokol Corporation (RSRM manufacturer) team soon narrowed the probable cause to a temporary nozzle restriction due to slag expulsion. In support of the team, Rockwell Aerospace performed fluid finite element simulations and vehicle flight dynamic correlations to investigate possible slag expulsion mechanisms responsible for pressure perturbations. Results of the simulations and analyses provided evidence that the combination of flight induced accelerations acting on accumulated slag and nozzle vectoring were the most probable cause of RSRM slag expulsion.

INTRODUCTION

During the STS-54 Space Shuttle mission, a 13 psi pressure perturbation was observed at approximately 68 seconds (Figure 1). Pressure perturbations have been experienced throughout the Shuttle program, with the largest usually occurring in the 65-80 second time period. The STS-54 right RSRM perturbation was not the largest experienced, however, since the left RSRM delivered slightly lower than nominal thrust at the time of the perturbation, the resulting thrust imbalance fell outside of flight experience (Figure 2).

During initial investigations of the perturbation, the cause was narrowed to temporary bore and/or nozzle restriction resulting in an associated pressure rise. The most likely scenarios were castable inhibitor failure and slag expulsion. Parallel studies were conducted to study the two scenarios. The castable inhibitor failure scenario, which theorized that a large section of failed inhibitor traveled down the bore at a velocity lower than the core flow, was soon dismissed as a result of Finite Element Analyses (FEA) and the lack of physical evidence found during post-test and post-flight hardware inspections. Although slag expulsion then became the most likely scenario, triggering mechanisms and processes for slag entrainment into the nozzle were not obvious.

In an effort to understand the phenomenon, a team of Rockwell Aerospace engineers experienced in solid rocket motors (SRM), FEA, Computational Fluid Dynamics (CFD), Shuttle trajectories, flight dynamics, and data analysis performed a detailed study.

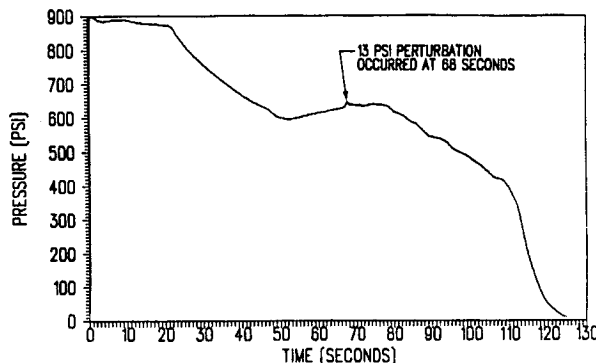


Fig 1. STS-54 Right RSRM Chamber Pressure

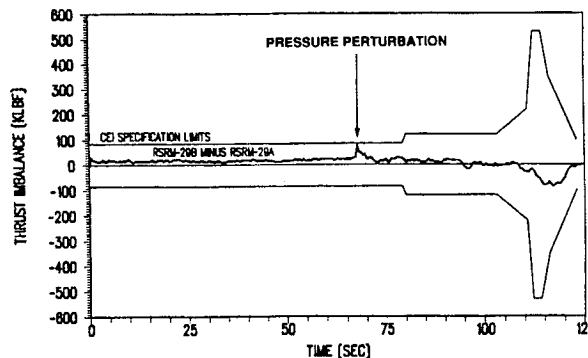


Fig. 2 STS-54 Thrust Imbalance

SLAG EXPULSION SCENARIO

Slag is a natural by-product from the combustion of aluminum and ammonium perchlorate. During a typical RSRM firing, over 300,000 pounds of slag are produced, entrained in the combustion gases, and expelled through the nozzle. The slag expulsion scenario proposed that a large quantity of slag, if suddenly expelled through the nozzle, could cause throat area reduction and subsequent pressure increase.

Initial evidence that slag expulsion was responsible for the pressure perturbations was obtained by analysis and correlation of RSRM static test data. Figure 3 shows Qualification Motor static test QM-8 chamber pressure (Figure 3a) and nozzle accelerometer responses (Figures 3b-d). It can be observed that the QM-8 pressure perturbations correlate in time to increased activity in the nozzle region corresponding to nozzle vectoring. It was believed that nozzle vectoring in the horizontal tests caused an asymmetrical internal flow pattern which swept large quantities of accumulated slag out of the nozzle. This theory was later confirmed with high-speed infra-red photography which captured the images of glowing slag in the bottom portion of the plume during nozzle vectoring events.

Even though the QM-8 data provided initial evidence that slag expulsion could cause pressure perturbations, it did not explain how large quantities of slag could be suddenly expelled from the RSRM during flight. There are two primary differences between static tests and flight concerning the slag scenario. First, since the RSRM is horizontal during static tests, the acceleration vector is perpendicular to the RSRM bore (gravity). In flight, however, acceleration is almost parallel to the bore (thrust). Since the orientation of the acceleration vector effects how slag is accumulated, the proximity to the nozzle of a significant slag pool cannot be assumed to be the same during flight as during static testing. Secondly, nozzle vectoring events are much more severe during static tests than any experienced in flight.

The RSRM design incorporates a submerged nozzle which provides a cavity aft of the internal nozzle lip and burning propellant. It was theorized that the cavity could become a reservoir for a large amount of slag captured under the influence of acceleration and combustion gas flow during flight. Slag production and aft cavity volume are more than sufficient to account for the expulsion quantities required to cause observed perturbations, however, mechanisms which could cause large quantities of slag to rise over the submerged nozzle lip in the 65-80 second time period had not been identified.

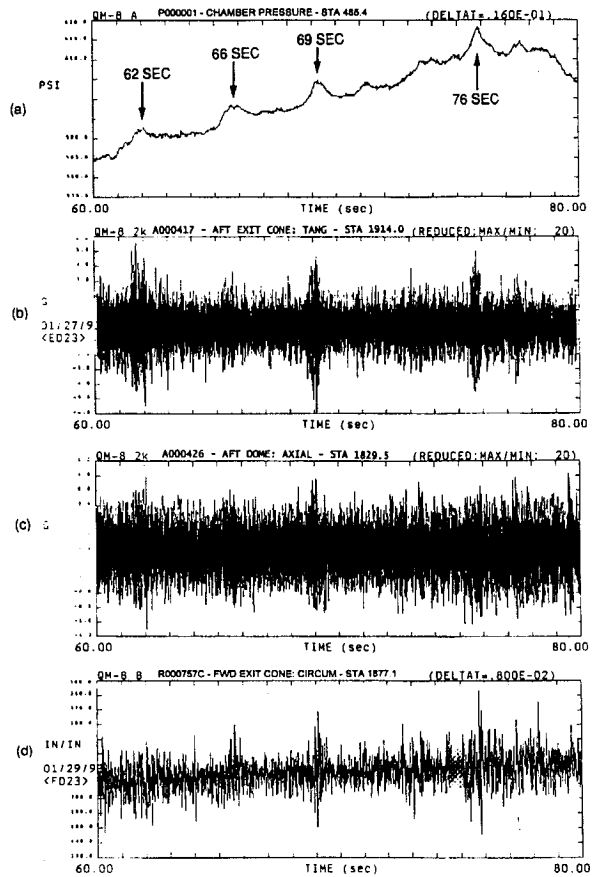


Fig. 3 QM-8 Static Test Data

SLAG SLOSHING

The first potential slag expulsion mechanism studied was sloshing. Sloshing was believed to be a plausible scenario after real-time radiography of a Titan motor firing showed captured slag to possess fluid-like behavior. Several fluid finite element models were developed to investigate whether flight dynamics could sufficiently excite slag sloshing modes. Models verified by closed-form analytical solutions resulted in the selection of EAL/SPAR finite element software for the study. In addition to fluid modeling accuracy, EAL/SPAR allowed direct application of dynamic input or forcing functions to the fluid elements. Figure 4 shows the RSRM aft dome model developed to simulate the cavity and accumulated slag.

A normal modes analysis on the FEM predicted a slag pool sloshing frequency of approximately 0.2 - 0.5 Hz. Flight specific slosh frequency is primarily dependent upon the cavity geometry and the magnitude of the acceleration normal to the free surface of the fluid.

SPACE SHUTTLE SOLID ROCKET MOTOR SLAG EXPULSION MECHANISMS

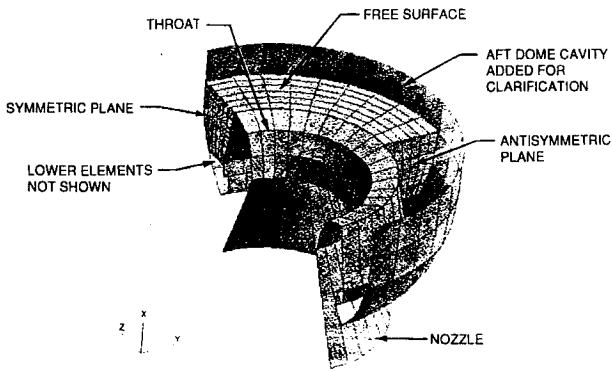


Fig. 4 RSRM Aft Cavity Finite Element Model

STS-54 flight accelerometer data was then applied to the FEM to assess potential slosh amplitudes versus time. Figure 5 shows how the FEM slosh response significantly increased at approximately 70 seconds when the lateral acceleration data was applied to the model. Figure 6 shows the amplitude vs. frequency vs. time history of the STS-54 lateral acceleration, revealing the energy increase in the 0.2 to 0.5 Hz range.

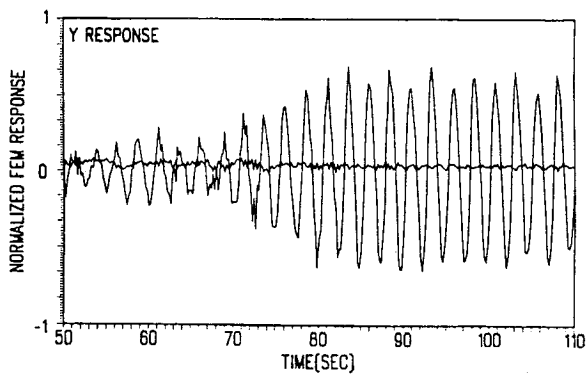


Fig. 5 STS-54 FEM Dynamic Response

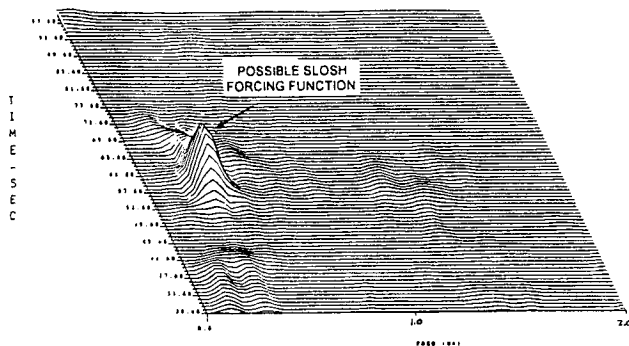


Fig. 6 STS-54 Lateral Acceleration

The characteristics of slag sloshing suggested by the FEM prompted a search for evidence of similar characteristics in other RSRM chamber pressure traces. Analyses revealed several pressure traces which exhibited sloshing characteristics. The best example occurred on STS-44. Figure 7 shows the STS-44 left RSRM chamber pressure trace and the three large perturbations which occurred 1.8 seconds apart. Figure 8 shows the correlation between STS-44 lateral acceleration and pressure perturbations. The lateral acceleration was digitally filtered to pass the 0.2 - 0.5 Hz band, as predicted by the FEA, and then a one-point RMS was performed for comparison to the chamber pressure. The comparison shows that the first perturbation occurred just after the large increase in acceleration and that all three perturbations are exactly correlated to the acceleration peaks with a small time lag between perturbations and acceleration peaks. The lag would correspond to the amount of time necessary for the slag to respond to the acceleration plus the time necessary for the pressure transducer at the head-end of the motor to respond to the throat restriction at the nozzle. Also, since the successive perturbations correlated with each half-cycle of the lateral acceleration trace, it suggested that slosh induced slag expulsion had occurred on both sides of the submerged nozzle in the yaw plane.

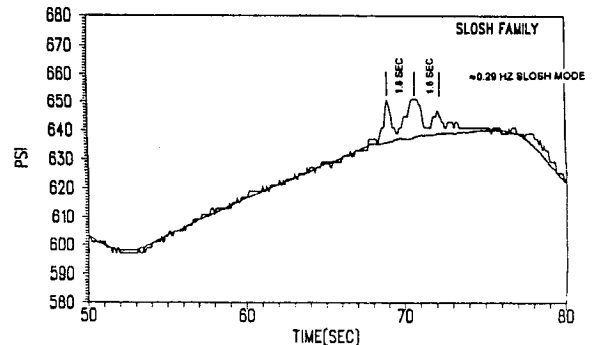


Fig. 7 STS-44 Left RSRM Chamber Pressure

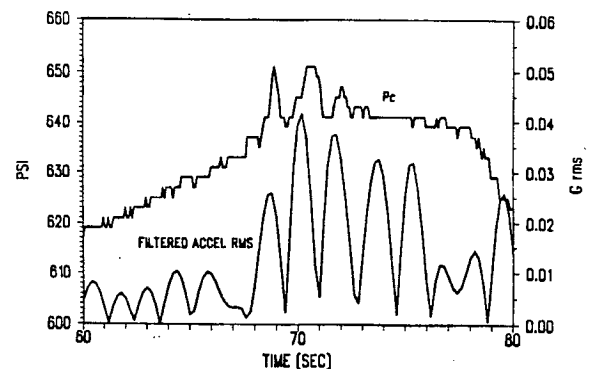


Fig. 8 STS-44 Pc Correlation to Acceleration

Figures 9 and 10 show other examples of multiple perturbations separated by times consistent with the predicted slosh frequency range. This evidence of slag sloshing and side-to-side expulsion is significant because it indicates that slag expulsion essentially shuts off on one side of the nozzle before initiating additional expulsion on the other side, thus providing a perturbation amplitude and duration limit. Figure 11 demonstrates this principal.

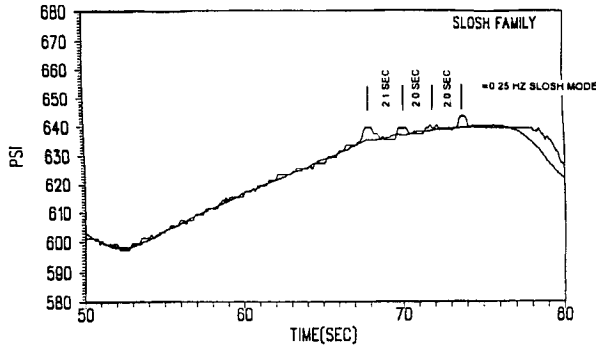


Fig. 9 STS-45 Left RSRM Chamber Pressure

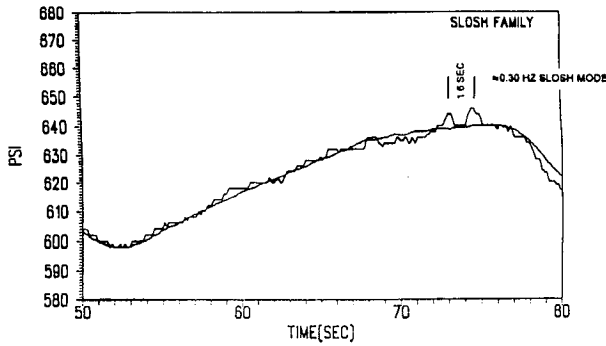


Fig. 10 STS-46 Left RSRM Chamber Pressure

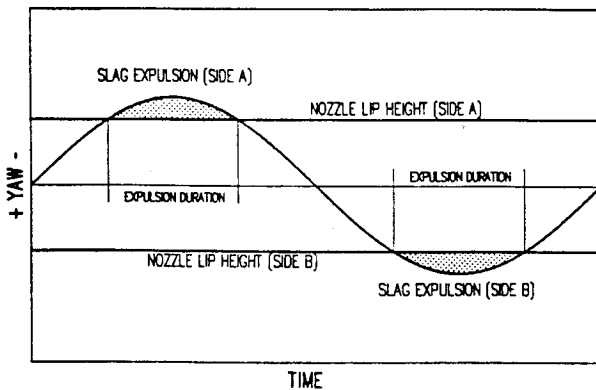


Fig. 11 Slosh Expulsion Limit

SLAG SPILLING

In addition to short, time consistent perturbations associated with sloshing, flight chamber pressure traces were also identified which deviated from nominal for long time durations (> 2 seconds), inconsistent with predicted slosh characteristics. By this time in the investigation, the MSFC team had acquired a wealth of data which proved pressure perturbations were a result of slag expulsion and no other phenomena were left on the fault tree to explain the long duration perturbations. So, assuming that the long perturbations were also a result of slag expulsion, an investigation was initiated to identify additional mechanisms which might explain this phenomenon.

Since perturbation amplitudes are proportional to slag expulsion volumes, the responsible mechanism must provide a means to expel large volumes of slag over a prolonged time period. The unknown mechanism was referred to as "spilling". Figures 12 - 14 show examples of perturbations belonging to the spill family. Note that each spill-type perturbation is preceded by a period of decreased pressure relative to the mean RSRM chamber pressure. The cause of the pressure decrease has not been explained, but may be indicative of a period of increased slag accumulation, temporarily reducing the mean slag expulsion through the nozzle and resulting in a pressure decrease.

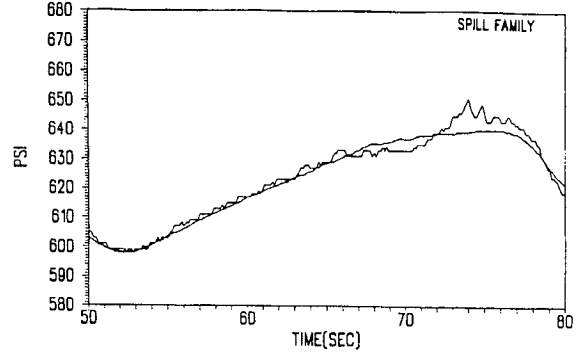


Fig. 12 STS-52 Right RSRM Chamber Pressure

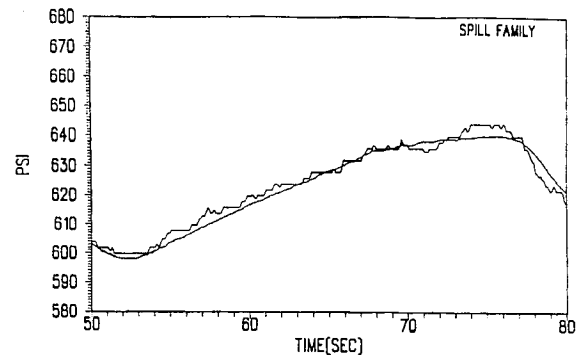


Fig. 13 STS-30 Right RSRM Chamber Pressure

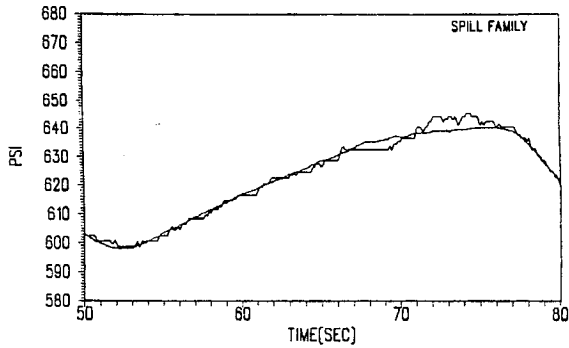
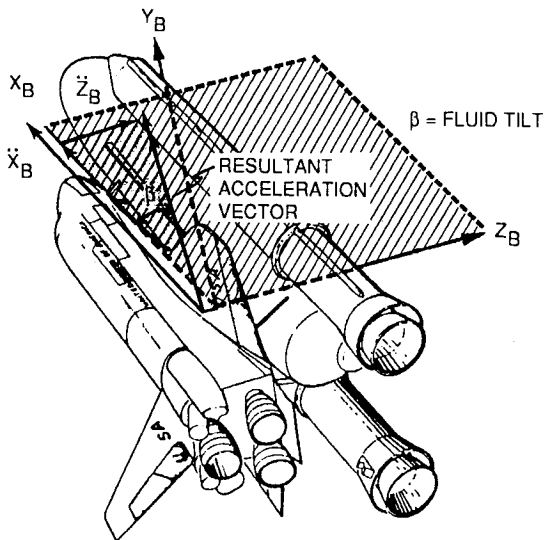


Fig. 14 STS-36 Left RSRM Chamber Pressure

The most plausible spill mechanism was thought to be trajectory induced and since the only sustained vehicle perturbation in the 65 - 80 second time period occurs during pitch maneuvers, analyses focused on pitch plane parameters. To determine the pitch influence, Shuttle yaw, pitch, and roll rate data were transformed to determine the time-varying vehicle orientation. The time-varying orientation was then compared to the time-varying total vehicle acceleration for correlation to chamber pressure traces (Figure 15).



RESULTANT ACCELERATION VECTOR WILL ALWAYS REMAIN IN THE POSITIVE QUADRANT AS SHOWN

Fig. 15 Vehicle Resultant Acceleration Vector

Assuming that the slag free surface is always perpendicular to the total acceleration vector, the angular difference between the RSRM centerline and the total acceleration vector results in a time-varying, relative expulsion potential referred to as "slag/nozzle proximity". A slag/nozzle proximity expulsion potential of 0 degrees means that the slag pool surface is perpendicular to the RSRM centerline and least likely

to be expelled. The potential for slag expulsion becomes more likely as slag/nozzle proximity values increase or decrease because the surface orientation change causes the slag pool to climb closer to the nozzle lip on one side or the other.

Analyses of RSRM flight data revealed significant changes in slag/nozzle proximity values. Also, the time period of the largest rate of change appears to correlate in time to observed spills. Large slag/nozzle proximity changes were found on all flights and is due to a rapid vehicle pitch maneuver after the Space Shuttle Main Engines return to flight power level after throttling through the area of maximum dynamic pressure. The rapid pitch maneuver causes the RSRM centerline to temporarily deviate from it's instantaneous acceleration vector and potential for sustained slag expulsion is highest. Figure 16 is typical of this phenomenon.

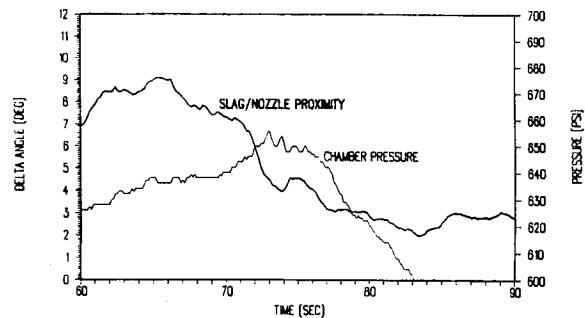


Fig. 16 STS-52 Pitch Plane Slag/Nozzle Proximity

RSRM NOZZLE VECTORING EFFECTS

Since the slosh and spill triggering mechanisms are present on all flights but large perturbations are relatively rare and have never occurred at the same time on both RSRMs, Rockwell began an investigation to identify additional contributors. Since rigid body vehicle parameters, motor performance, and internal environments would be expected to affect both motors similarly, nozzle vectoring appeared to be a likely candidate for further analysis.

A computer program was developed to perform Thrust Vector Control (TVC) conversions of all RSRM flight data for study and correlation to flight chamber perturbations. As shown in Figure 17, vectoring in the yaw plane is identical for both left and right RSRMs, however, the pitch plane vectoring is significantly different. The pitch plane vectoring differences are typical of all flights and differs depending on trajectory perturbations such as upper level winds. As far as slag expulsion is concerned, the opposing pitch plane vectoring has two primary effects. First, vectoring causes a tilting of the submerged nozzle lip inside the motor. The lowering of one side and lifting of the other side creates a preferential expulsion path for slag.

SPACE SHUTTLE SOLID ROCKET MOTOR SLAG EXPULSION MECHANISMS

Secondly, nozzle vectoring causes changes to the aft cavity geometry which can result in powerful circumferential flow forces. These flow forces, combined with nozzle tilt and vehicle dynamics, are potential factors causing differing slag expulsion events.

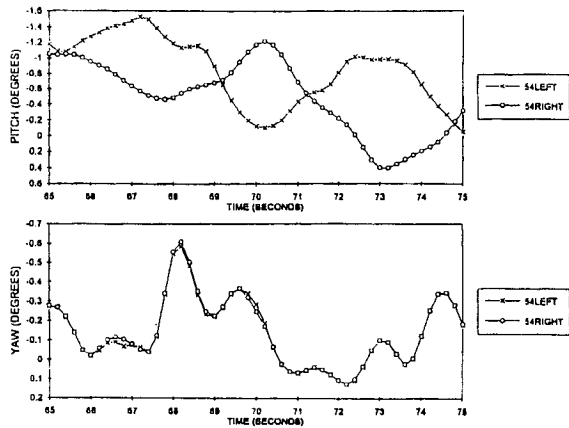


Fig 17 STS-54 Nozzle Vectoring Time History

Polar plots help visualize the time-varying nozzle vectoring for correlation with chamber pressure. Figure 18 is the vector polar plot of STS-44. Each point represents the nozzle vector angle at 0.2 second time increments from 65 to 72 seconds. The three STS-44 perturbations appear to correlate with yaw vectoring since each perturbation occurs near a yaw extrema. This data provides further evidence that the STS-44 perturbations were associated with yaw plane activity, as suggested by the slosh mechanism discussion earlier.

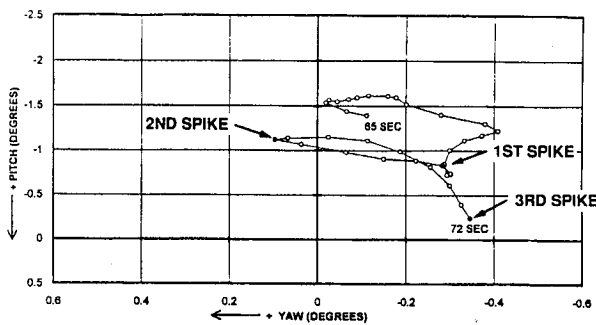


Fig. 18 STS-44 Left Nozzle Vectoring Time History

SUMMARY

Rockwell analyses identified slag expulsion mechanisms which explain observed chamber pressure perturbations. After extensive investigation by the MSFC team, no other slag expulsion mechanisms have been identified. Since all flights do not exhibit significant perturbations, even when all triggering

mechanisms are present, the occurrence of perturbations appears to a random phenomenon resulting from particular combinations of triggers. Also, regardless of which triggering mechanisms exist, significant slag accumulation must be present. Propellant blend variations appear to be a significant factor regarding slag accumulation. Results of these analyses have resulted in a better understanding of pressure perturbation and their cause, important to the current Space Shuttle program and future solid rocket propulsion systems.

ACKNOWLEDGMENTS

The work presented here was funded by NASA under Contract NAS8-38550 for the Marshall Space Flight Center. The author wishes to acknowledge the contributions provided by the MSFC/Thiokol Team including the RSRM Chief Engineer's office, F. M. Bugg of the MSFC Structures and Dynamics Laboratory, and ERC Inc.

The author also wishes to acknowledge the significant contributions provided by the Rockwell Huntsville Simulation/Analysis team including J. R. Hawkins, T. M. Lohrer, P. J. Mann, T.D. Reynolds, J. A. Wilbanks, D. B. Burnette, and J. B. Holt.